Journal of Materials Chemistry A

Accepted Manuscript

ROYAL SOCIETY OF CHEMISTRY

www.rsc.org/materialsA

Graphic TOC

"For Table of Contents Use Only"

Title: Novel triphenylamine functionalized bithiazole-metal complex with C_{60} for photocatalytic hydrogen production under visible light irradiation

Author: Jingpei Huo and Heping Zeng*

The resulting composite **6** (2.0 wt% C_{60}) is an efficient and fully recyclable catalyst for photocatalytic H_2 production (7.39 $mmol*h^{-1}*g^{-1}$) under visible light illumination.

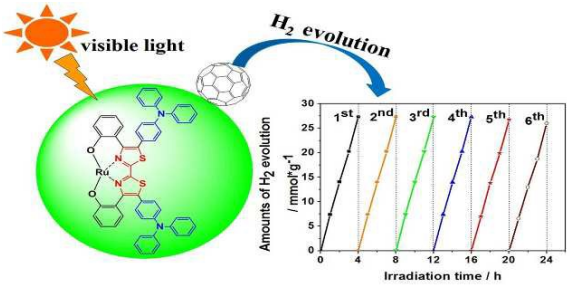

Cite this: DOI: 10.1039/c0xx00000x

www.rsc.org/xxxxxx

ARTICLE TYPE

Novel triphenylamine functionalized bithiazole-metal complex with C_{60} for photocatalytic hydrogen production under visible light irradiation

Jingpei Huo and Heping Zeng*

Received (in XXX, XXX) Xth XXXXXXXXX 20XX, Accepted Xth XXXXXXXXX 20XX

DOI: 10.1039/b000000x

A series of novel cost-effective nanocomposite photocatalysts containing triphenylamine functionalized bithiazole-metal complex and C_{60}, have been synthesized and systematically characterized. Those bithiazole-metal complexes with C_{60} serve both as a photosensitizer and a photocatalyst for hydrogen evolution under visible-light irradiation, and their photocatalytic activities are approximately 4-6 times higher than the corresponding complexes.

Photocatalytic hydrogen (H_2) production from water splitting under visible light irradiation has been receiving a surge of interests.[1-5] Intensive efforts have been directed towards photocatalytic H_2 generation using semiconductor-based photocatalysts,[6-10] or metal (M) complexes[11-14] as a chromophore/catalyst.[15, 16] As a kind of porous materials,[17] M complexes containing porphyrin, phthalocyanine, aminoterephthalate or poly-pyridine, have been recognized as potential candidates as photocatalysts.[18, 19] Unfortunately, problems plaguing these M-complexes include insufficient reactivity and low stability.[20, 21] Hence, there is an ever-growing need for the improvement of their activities and durabilities.

It is well known that many molecules possessing bithiazole moiety are ideal chromophores[22] because they absorb strongly in the visible region[23] and have been shown to transfer energy and electrons to acceptor sites with high efficiencies.[24] Especially, an attractive feature of bithiazole is used for precursor of these M-complex molecular conductors, exhibiting semiconducting behavior.[25, 26] Recently, increasing attention has been attached to expand the thiazole-based system, such as triphenylamine (TPA) and other electron-donating groups.[27, 28] Broadly speaking, TPA and its derivatives have been widely used as donors for construction of hole-transport materials,[29, 30] but also demonstrated promising properties in photo-induced electron transfer and charge separation.[31] Based on the richness of hole-transport properties, it is easy to adjust light absorption and improve the efficiency of the intramolecular charge separation, thereby initiating desirable photocatalytic properties for specific applications in photocatalytic H_2 production.[32, 33]

Fullerene (C_{60}) is the most symmetrical and stable carbonaceous material, rather than graphene, carbon nanotube, graphite.[34, 35] Besides, the long-range π-conjugation of C_{60} endows it with superior and unique properties, including high specific surface area, exceptional electrical conductivity and electron mobility.[36, 37] Due to its remarkable nature, C_{60} has been reported to be an excellent cocatalyst for the enhancement of photocatalytic performances of metal complexes, which effectively facilitates charge separation and suppresses recombination of photoexcited electron-hole pairs.[38, 39] However, to the best of our knowledge, there is no reported investigation focused on the photocatalytic activity of triphenylamine functionalized bithiazole (2TPABTz)-metal complex composites. Herein, according to our previous research,[40-43] a variety of 2TPABTz-based M-complexes including copper (Cu), cobalt (Co), ruthenium (Ru) and the corresponding nanocomposites **1-6** were simultaneously synthesized (**Scheme S1**). Their structures and properties are characterized by UV-vis and photoluminescence (PL) spectroscopies, transmission electron microscopy (TEM), energy dispersive X-ray spectroscopy (EDX), X-ray diffraction (XRD), elemental analysis, X-ray photoelectron spectroscopy (XPS), Raman spectra, Brunauer-Emmett-Teller (BET), transient photocurrent response and electrochemical impedance spectra (EIS) analysis. Furthermore, their photocatalytic activities are investigated under visible-light illumination.

The experimental UV-Vis absorption spectra of all the as-synthesized samples **1-6** were recorded at room temperature, as given in **Fig. 1**. Their absorption spectra were featured by the most intense absorption bands in the ultraviolet region at wavelengths below 350 nm (**Fig. 1**), arising from the spin-allowed π-π* transition localized on coordinated aromatic ligands within each complex. The next, weaker, broad band, which reaches approximately 430 nm into the visible region, can be ascribed to the metal-to-ligand charge-transfer (MLCT) transition.[44] On the other hand, the Soret bands in 2TPABTz-core have been found in the absorption spectra of nanocomposites **4-6** is red-shifted and become strong compared with those complexes **1-3** (**Fig. 1**), which is beneficial to absorbing the solar radiation, because the introduction of C_{60} would extend π-conjugation, strengthening the intensive electronic interaction between M complex and nanostructured carbon when C_{60} is used as carbon resource.[45]

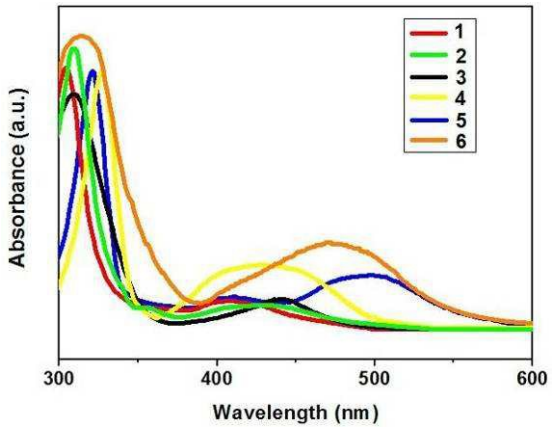

Fig. 1 Absorption spectra of 2TPABTz-based M complexes and the corresponding nanocomposites **1-6**.

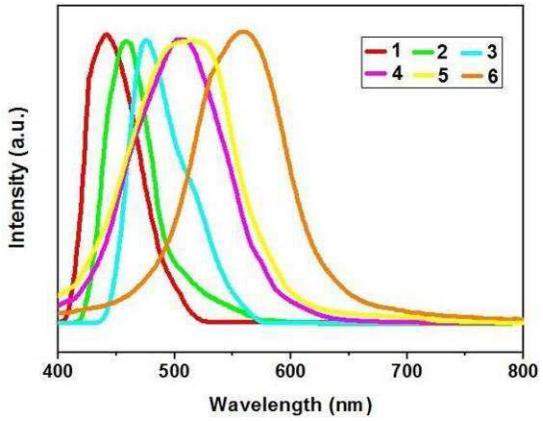

Fig. 2 Emission spectra of 2TPABTz-based M complexes and the corresponding nanocomposites **1-6**.

The normalized luminescence spectra of these samples **1-6** in their solid state at ambient air and room temperature are presented in **Fig. 2**, and the corresponding photophysical data are collected in **Table 1**. The emission peak maximum ranges from 442 to 561 nm, and their color shifts depended on the organic ligand chromophores with the difference in the ligand field strength.[44, 46] Obviously, the emission peak maximum of complex **3** was the biggest one among the three complexes **1-3**, owing to the increased effective conjugation length of ligands in complex **3**. Interestingly, the apparent bathochromic shift reflects the strong electronic coupling between the M-complex and C_{60}.[47] The composite **6** shows a broad, structureless emission band, indicating that the emission can be attributed to the prevalent MLCT state. A similar trend was observed for the samples **1-6** with quantum yields (Φ) and summarized in **Table 1**. The samples **3** and **6** give strong fluorescence at 475 nm (Φ = 53.8%) and 561 nm (Φ = 82.5%), respectively.

To study the spectral features of the hybrids **1-6**, time-resolved fluorescence decay profile measurements were carried out, and their excited-state lifetimes (τ) were listed in **Table 1**.[48] The fluorescence lifetime of complex **3** is much longer than those of complex **1** and **2**. The results suggest that complex **3** might provide a more stable environment for the excited state.[49] While for another three ones, all of them show a bi-exponential decay function with a shorter lifetime and a longer lifetime. The shorter-lifetime was indicative of electron transfer from the metal core to 2TPABTz. And the longer decay component can provide the long-lived electron in the system of composite, clearly illustrating the incorporation of C_{60} can promote the interfacial charge transfer process, and thus the rate of hydrogen production may be improved.[48]

Table 1 Spectroscopic properties of 2TPABTz-metal complexes and the corresponding nanocomposites **1-6**

Sample	λ_{em} (nm)[a]	Φ (%)[b]	τ_1 (ns)[c]	τ_2 (ns)[c]
1	442	44.7	1.48	-
2	458	49.1	2.01	-
3	475	53.8	3.93	-
4	505	74.9	3.53	9.82
5	513	61.3	2.98	7.56
6	561	82.5	4.57	18.11

[a]Recorded at room temperature, and excited at 415 nm.

[b]The solid fluorescence quantum yields (Φ) were measured on a calibrated integrating sphere system (λ_{ex} = 415 nm).

[c]Fluorescence lifetime.

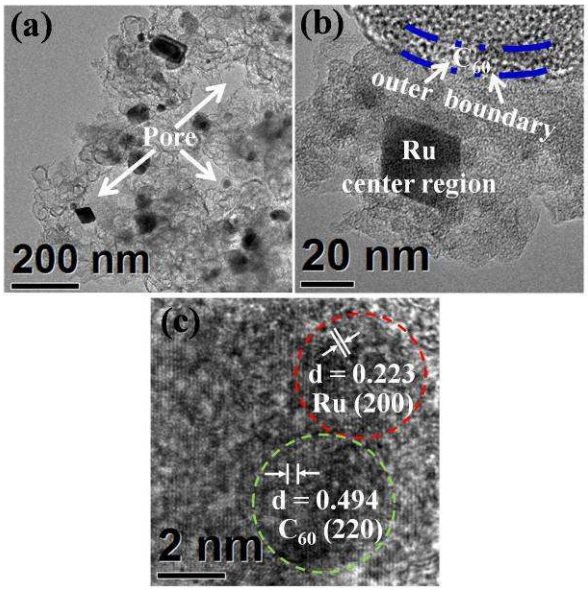

Fig. 3 TEM and HR-TEM images of composite **6**.

TEM analyses were used to further characterize the microstructure of composite **6**, and illustrated on **Fig. 3**. **Fig. 3a** displays the morphology of the resulting composite **6**, forming irregular granules. The size of composite **6** has a range from 50 to 80 nm. It is favourable for photoelectrons transiting to the surface, leading to an increase of the reaction activities.[50] Noticeably, there are some lattice fringes in the outer boundary, which may be C_{60} molecules on **Fig. 3b**. And it also shows that C_{60} clusters in the system are attached on the composite **6** sidewall indicated by the white arrows, which is similar to the previous report.[51] As shown in **Fig. 3c**, HR-TEM study confirmed that the center region was still Ru with a lattice spacing of 0.223 nm for the (200) plane, and the outside layer had a cubic phase fullerene structure with a lattice spacing of 0.494 nm for the (220) plane.[52]

Additionally, the chemical composition of the sample was determined by EDX. The EDX spectrum (**Fig. 4**) confirms that the sample consists of C, O, Ru, N and S elements, as expected. The EDX result reveals that composite **6** can be detected in an area with random selection. This manifests that these composites overspread on the surface of C_{60} evenly, which is in agreement with the elemental mapping patterns. There are some small impurities, which are believed to have been introduced into the composite **6** using the C_{60} without purification. Meanwhile, carbon and ruthenium are present as major elements with small quantities of oxygen.[52]

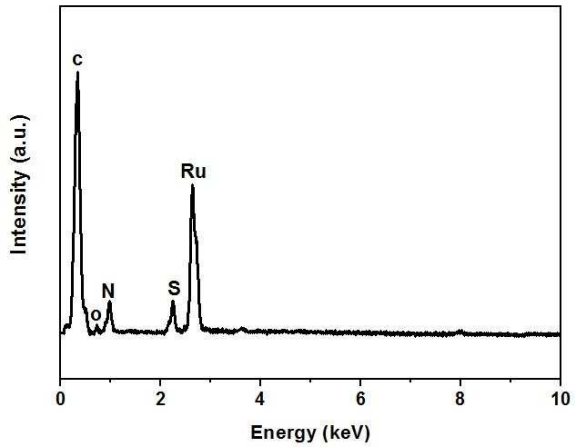

Fig. 4 EDX spectra of composite **6**.

XPS measurements were performed to elucidate the composite **6**. As expected, it was found to be that composite **6** contained Ru, S, N, O, and C, with sharp XPS peaks centered at binding energies of 532.72 (O 1s), 487.29 (Ru 3p), 400.43 (N 1s), 284.25 (C 1s), and 164.38 (S 2p).[53] To further analyze the chemical nature of composite **6**, the high-resolution XPS spectrum was examined (**Fig. S13**). And it revealed three prominent peaks at 284.25 ev, 282.21 eV, and 285.48 eV, which are assigned to C (1s), Ru ($3d_{5/2}$) and Ru ($3d_{3/2}$) respectively, evidencing the successful immobilization of the ruthenium complex on the C_{60} support in the composite **6** system.[54]

The Raman spectral data of pure fullerene and composite **6** are shown in **Fig. S14**. There are two typical Raman peaks of C_{60} located at 1465 and 1582 cm^{-1}, which belong to the A_g and H_g mode of C_{60}, respectively.[55] It was clear that the other bands of C_{60} disappeared, except a major band (A_g) at 1465 cm^{-1} (**Fig. S14**). Further observation showed that after C_{60} was hybridized with composite **6**, the A_g symmetry band at 1465 cm^{-1} was slightly downshifted and broadened. This phenomenon demonstrated that the A_g pentagonal pinch mode was related to the carrier transfer.[56]

The BET specific surface area (S_{BET}) and pore structure of the as-prepared samples **1-6** are investigated using adsorption desorption measurements. **Table 2** shows quantitative details on BET specific surface area, pore volume and average pore size of those samples, and there is a difference among them. It can be seen that composite **6** showed the highest S_{BET} of all the six ones. The larger surface area of the nanocomposites can supply more surface active sites and make charge carriers transport easier, resulting in an enhancement of the photocatalytic performance.[20] In the meantime, the results are obtained according to the corresponding pore size distribution. As summarized in the **Table 2**, this latter observation was shown that composite **6** has the largest surface area and pore size, indicating the presence of mesopores. These datum illustrate that C_{60} could introduce porous structure with increased surface area, which is helpful for enhancing the photocatalytic activity.[57, 58]

Photocatalytic activity of various samples was quantitatively evaluated by photocatalytic H_2 evolution from the suspension of photocatalysts in an aqueous lactic acid (LA) solution for 4 h using visible-light irradiation (>420 nm), and given in **Fig. 5** and **Table 2**. Before the actual photocatalytic experiment was performed, control experiments were taken by a pure LA solution in the absence of either a photocatalyst or irradiation. No appreciable H_2 evolution was detected, indicating that H_2 was produced from the LA solution by photocatalytic reactions on a photocatalyst.[59] **Fig. 5a** and **Table 2** show the hydrogen production rate of the as-synthesized photocatalysts **1-6** and P25, separately. As can be seen, a much more efficient H_2 production was achieved with complex **3** (0.98 $mmol*h^{-1}*g^{-1}$) compared to other complexes, which can be also ascribed to two reason. One is the extended π-conjugated structure of complex **3**, which may harvest irradiation light in a wider range, matching with the upper absorption spectra.[60] Another one is the efficient interfacial electrons transfer between photoexcited 2TPABTz and Ru core in the system also enhances separation efficiency of photoexcited carriers as well as photocatalytic activity.[61] After loading C_{60} cocatalyst, all the three composites exhibit a surprisingly enhanced photocatalytic activity for hydrogen evolution reaction. The composite **6** produced 6.12 $mmol*h^{-1}*g^{-1}$, which is about 1.5 times higher than that of composite **4** and **5**. At the presence of C_{60}, it is greatly favorable to the H_2 production, functioning as an electron reservoir to transfer, separating electrons and holes.[38, 39, 50] Moreover, the apparent quantum efficiency (QE) of all investigated photocatalysts is also listed in **Table 2**, and it is noteworthy that composite **6** obtained the biggest QE value of 4.27% at 420 nm.

On the other hand, **Fig. 5b** shows the rate of H_2 evolution of composite **6** with different weight amounts of C_{60} cocatalyst. It can be seen that the composite **6** with 2.0 wt% content of C_{60} cocatalyst shows the highest hydrogen production rate of 7.39 $mmol*h^{-1}*g^{-1}$. Preliminary studies revealed that C_{60} could promote the transfer of the photogenerated electrons in the conduction band of catalysts to the edges of composite **6** and then react with adsorbed H^+ to form H_2.[51] In addition, the high concentration of electrons between the composite **6** layer and the C_{60} layer could greatly enhance the electronic conductivity of composites, and therefore the cocatalytic activities of composites are increased significantly.[62] Whereas a further increase in the C_{60} content leads to a significant decrease in photocatalytic activity, which may be attributed to increased absorbance and scattering of photons through excess C_{60} in the photo system.[63] Consequently, the composite **6** (2.0 wt% C_{60}) was the best performing photocatalyst and chosen for the following

recycling experiments.

Furthermore, the repeatability of composite **6** (2.0 wt% C_{60}) was tested in six consecutive runs of accumulatively 24 h under the same conditions (**Fig. 5c**). After six recycles, no deactivation of that catalyst occurs in the repeated use, implying that it exhibits good stability and reusability. It has been proved that the nanocomposite **6** was not photo-corroded and suitable for hydrogen generation from LA aqueous solution.[50]

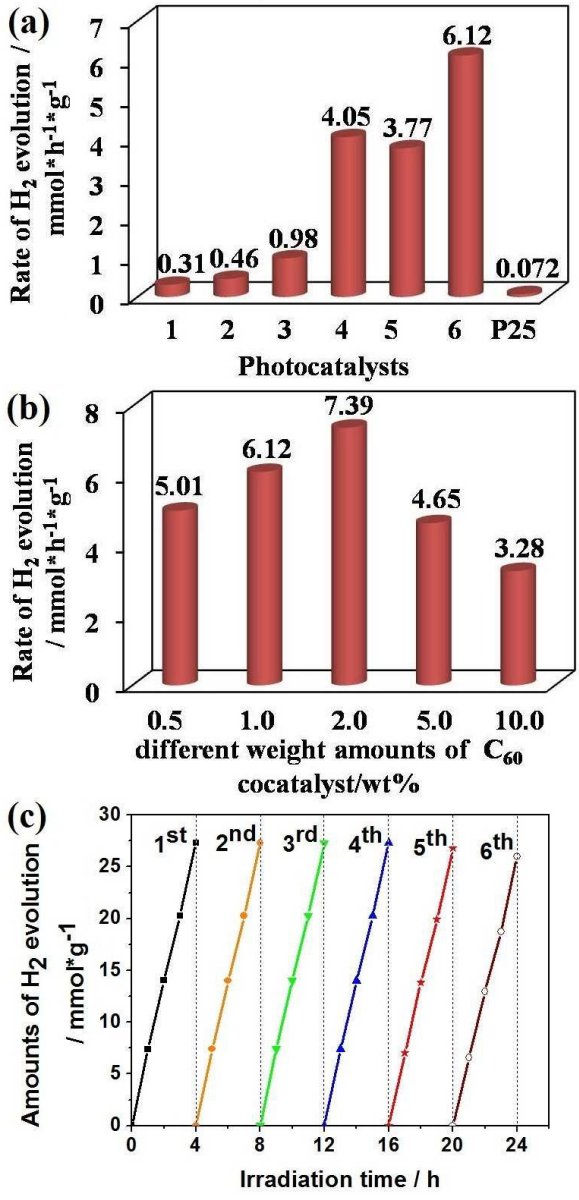

Fig. 5 Photocatalytic activity of the investigated samples (0.05 g) in an aqueous solution (100 mL) containing LA (10 mL) under visible light illumination: (a) hydrogen evolution rate of as-synthesized samples **1-6** and P25, respectively (irradiation time = 4 h); (b) the rate of H_2 evolution of composite **6** with different weight amounts of C_{60} cocatalyst (irradiation time = 4 h); (c) cycling test of photocatalytic H_2 generation for composite **6** (2.0 wt% C_{60}, irradiation time = 24 h).

Table 2 The physicochemical properties, hydrogen production rate and QE of as-prepared photocatalysts **1-6** and P25.

Sample	S_{BET} (m^2*g^{-1})	Pore volume (cm^3*g^{-1})	Average pore size (nm)	H_2 ($mmol*h^{-1}*g^{-1}$)[a]	QE (%)[b]
1	24.9	0.14	7.5	0.31	0.08
2	31.5	0.17	8.6	0.46	0.14
3	47.3	0.29	11.9	0.98	0.39
4	103.1	0.82	19.4	4.05	3.06
5	95.4	0.71	16.7	3.77	2.51
6	129.8	1.14	23.8	6.12	4.27
P25[41]	45.2	0.23	10.3	0.072	0.04

[a]Reaction was conducted under a 300 W Xe arc lamp with a ultraviolet cut-off filter; 0.05 g of each catalyst was dispersed in the above conditions.

[b]QE was calculated with the amounts of H_2 evolution under monochromatic light illumination (λ = 420 nm) in 1 h.

In particular, a comparison of the XRD patterns of the composite **6** (2.0 wt% C_{60}) before and after stability test is presented in **Fig. S16**. For comparison, there is no obvious changes and intensities in the locations of these peaks, suggesting that it has considerable photostability.[51, 64] Moreover, it can be found that there are negligible variations at the surface element composition of composite **6** before and after six cycles of photocatalytic hydrogen evolution tests in **Table S1**. It is indicated that no new bond evolved in composite **6**. The formed heterojunction at the interface is beneficial for the accelerated charge separation and improved photocatalytic activity.[65-68]

To provide additional evidence for the above experiment, the transient photocurrent responses are recorded for the **4-6** and P25 sample electrodes.[62, 63] **Fig. 6** shows the *I-t* curves for all the film electrodes with several on-off cycles, under intermittent visible light illumination (420 nm). Apparently, the photocurrent value rapidly decreases to zero as soon as the light turns off, and it returns to be a constant when the light is on again, exhibiting a good repeatability. Composite **6** photoelectrode showed the biggest value, which achieved about 2.5, 4 and 10 times as high as that of the composite **4**, **5** and P25, respectively. It is noted to be that smaller recombination and more efficient carrier separation at the composite **6** interface.[58]

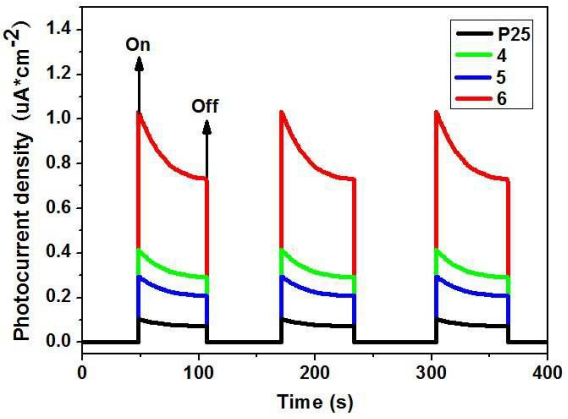

Fig. 6 The transient photocurrent responses of the composites **4-6** and P25 under chopped light illumination of 420 nm at 0.5 V bias *vs.* Ag/AgCl.

Besides, EIS analysis is an appropriate technique to study

the charge transfer process occurring in a three-electrode system.[58, 69, 70] **Fig. 7** displays the EIS Nyquist plots of the composites **4-6** and P25 samples. The observed semicircles correspond to the charge transfer resistance at the sample-electrode interface. The smaller the semicircle arc is, the easier is the charge transfer.[71] As can be seen from **Fig. 7**, the composite **6** shows the smallest semicircle in the middle-frequency region, in comparison to the five other ones, implying that the lower resistance and the faster interfacial charge transfer.[71] This is consistent with the upper photocurrent results.

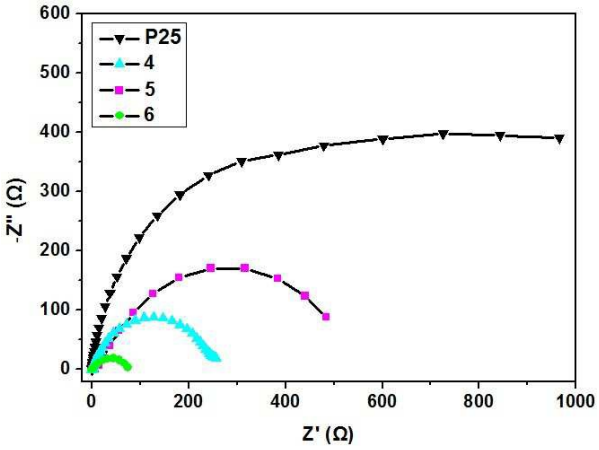

Fig. 7 EIS of the composites **4-6** and P25.

In summary, a range of photocatalysts **1-6** were synthesized successfully and characterized. Through the optimizing of each component proportion, the best photocatalytic performance is observed for composite **6** (2.0 wt% C_{60}). And also, it exhibits an exceptionally high rate of hydrogen production at 7.39 $mmol*h^{-1}*g^{-1}$ under visible light illumination, and shows relatively high reusability. More importantly, this work not only offers a stable and efficient nanocomposite photocatalyst but also sheds new inroads for engineering cost-effective nanocomposites, which could open up new insights to promote the improvement of photocatalytic conversion efficiency for metal complex.

Acknowledgements

We are grateful to the National Natural Science Foundation of China (No. 21371060) and the research fund of the Key Laboratory of Fuel Cell Technology of Guangdong Province for financial support.

Notes and references

State Key Laboratory of Luminescent Materials and Devices, Institute of Functional Molecules, School of Chemistry and Chemical Engineering, South China University of Technology, Guangzhou, 510641, P. R. China. Fax: 86-20-87112631; Tel: 86-20-87112631; E-mail: hpzeng@scut.edu.cn.

† Electronic Supplementary Information (ESI) available: Experimental details, Figures and so on. See DOI: 10.1039/b000000x/

1 J.-X. Jian, Q. Liu, Z.-J. Li, F. Wang, X.-B. Li, C.-B. Li, B. Liu, Q.-Y. Meng, B. Chen, K. Feng, C.-H. Tung and L.-Z. Wu, *Nature Chem.*, 2014, **4**, 2695.

2 R. B. Jiang, B. X. Li, C. H. Fang and J. F. Wang, *Adv. Mater.*, 2014, **26**, 5274.

3 L. Liao, Q. H. Zhang, Z. H. Su, Z. Z. Zhao, Y. N. Wang, Y. Li, X. X. Lu, D. G. Wei, G. Y. Feng, Q. K. Yu, X. J. Cai, J. M. Zhao, Z. F. Ren, H. Fang, F. Robles-Hernandez, S. Baldelli and J. M. Bao, *Nature Nanotech.*, 2014, **9**, 69.

4 D. J. Martin, K. P. Qiu, S. A. Shevlin, A. D. Handoko, X. W. Chen, Z. X. Guo and J. W. Tang, *Angew. Chem. Int. Ed.*, 2014, **53**, 9240.

5 Z. J. Han, F. Qiu, R. Eisenberg, P. L. Holland and T. D. Krauss, *Science*, 2012, **338**, 1321.

6 S. Bai, J. Ge , L. L. Wang, M. Gong , M. S. Deng, Q. Kong, L. Song, J. Jiang, Q. Zhang, Y. Luo, Y. Xie and Y. J. Xiong, *Adv. Mater.*, 2014, **26**, 5689.

7 J. Zhang , L. F. Qi, J. R. Ran, J. G. Yu and S. Z. Qiao, *Adv. Energy Mater.*, 2015, *in press* (10.1002/aenm.201301925).

8 R. Su, R. Tiruvalam, A. J. Logsdail, Q. He, C. A. Downing, M. T. Jensen, N. Dimitratos, L. Kesavan, P. P. Wells, R. Bechstein, H. H. Jensen, S. Wendt, C. R. A. Catlow, C. J. Kiely, G. J. Hutchings and F. Besenbacher, *ACS Nano*, 2014, **8**, 3490.

9 M. Y. Wang, J. Ioccozia, L. Sun, C. J. Lin and Z. Q. Lin, *Energy Environ. Sci.*, 2014, **7**, 2182.

10 M. Behrens, F. Studt, I. Kasatkin, S. Kühl, M. Hävecker, F. Abild-Pedersen, S. Zander, F. Girgsdies, P. Kurr, B.-L. Kniep, M. Tovar, R. W. Fischer, J. K. Nørskov and R. Schlögl, *Science*, 2012, **336**, 893.

11 M. A. Nasalevich, R. Becker, E. V. Ramos-Fernandez, S. Castellanos, S. L. Veber, M. V. Fedin, F. Kapteijn, J. N. H. Reek, J. I. van der Vlugt and J. Gascon, *Energy Environ. Sci.*, 2015, **8**, 364.

12 T. Stoll, M. Gennari, J. Fortage, C. E. Castillo, M. Rebarz, M. Sliwa, O. Poizat, F. Odobel, A. Deronzier and M.-N. Collomb, *Angew. Chem. Int. Ed.*, 2014, **53**, 1654.

13 L.-Z. Wu, B. Chen, Z.-J. Li and C.-H. Tung, *Acc. Chem. Res.*, 2014, **47**, 2177.

14 R. E. Rodríguez-Lugo, M. Trincado, M. Vogt, F. Tewes, G. Santiso-Quinones and H. Grützmacher, *Nature Chem.*, 2013, **5**, 342.

15 R. S. Khnayzer, V. S. Thoi, M. Nippe, A. E. King, J. W. Jurss, K. A. El Roz, J. R. Long, C. J. Chang and F. N. Castellano, *Energy Environ. Sci.*, 2014, **7**, 1477.

16 K. Kitamoto, K. Sakai, *Angew. Chem. Int. Ed.*, 2014, **53**, 4618.

17 N. Linares, A. M. Silvestre-Albero, E. Serrano, J. Silvestre-Albero and J. García-Martínez, *Chem. Soc. Rev.*, 2014, **43**, 7681.

18 Y. Ma, X. L. Wang, Y. S. Jia, X. B. Chen, H. X. Han and C. Li, *Chem. Rev.*, 2014, **114**, 9987.

19 U. Banin, Y. Ben-Shahar and K. Vinokurov, *Chem. Mater.*, 2014, **26**, 97.

20 M. Waki, Y. Maegawa, K. Hara, Y. Goto, S. Shirai, Y. Yamada, N. Mizoshita, T. Tani, W.-J. Chun, S. Muratsugu, M. Tada, A. Fukuoka and S. Inagaki, *J. Am. Chem. Soc.*, 2014, **136**, 4003.

21 Y. Y. Jiang, Y. Z. Lu, X. Y. Lv, D. X. Han, Q. X. Zhang, L. Niu and W. Chen, *ACS Catal.*, 2013, **3**, 1263.

22 K. Y. Liu, Y. Wen, T. Shi, Y. Li, F. Y. Li, Y.-L. Zhao, C. H. Huang and T. Yi, *Chem. Commun.*, 2014, **50**, 9141.

23 X. G. Guo, J. Quinn, Z. H. Chen, H. Usta, Y. Zheng, Y. Xia, J. W. Hennek, R. P. Ortiz, T. J. Marks and A. Facchetti, *J. Am. Chem. Soc.*, 2013, **135**, 1986.

24 F. Pammer, J. Jäger, B. Rudolf and Y. Sun, *Macromolecules*, 2014, **47**, 5904.

25 P. Bujak, I. Kulszewicz-Bajer, M. Zagorska, V. Maurel, I. Wielgus and A. Pron, *Chem. Soc. Rev.*, 2013, **42**, 8895.

26 N. Tenn, N. Bellec, O. Jeannin, L. Piekara-Sady, P. Auban-Senzier, J. Íñiguez, E. Canadell and D. Lorcy, *J. Am. Chem. Soc.*, 2009, **131**, 16961.

27 J. H. Kim, H.-S. Shim, H. Lee, M.-S. Choi, J.-J. Kim and Y. S. Seo, *J. Phys. Chem. C*, 2014, **118**, 11559.

28 K. Wang, S. Huang, Y. Zhang, S. S. Zhao, H. Y. Zhang and Y. Wang, *Chem. Sci.*, 2013, **4**, 3288.

29 Y. Im and J. Y. Lee, *Chem. Mater.*, 2014, **26**, 1413.

30 B. Xu, H. N. Tian, L. L. Lin, D. P. Qian , H. Chen, J. B. Zhang, N. Vlachopoulos, G. Boschloo, Y. Luo, F. L. Zhang, A. Hagfeldt and L. C. Sun, *Adv. Energy Mater.*, 2015, *in press* (DOI: 10.1002/aenm.201401185).

31 J. J. Wang, S. R. Wang, X. G. Li, L. F. Zhu, Q. B. Meng, Y. Xiao and D. M. Li, *Chem. Commun*., 2014, **50**, 5829.
32 H.-R. Fu, Y. Kang and J. Zhang, *Inorg. Chem*., 2014, **53**, 4209.
33 D. P. Hoffman, O. P. Lee, J. E. Millstone, M. S. Chen, T. A. Su, M. Creelman, J. M. J. Fréchet and R. A. Mathies, *J. Phys. Chem. C*, 2013, **117**, 6990.
34 T. E. Shubina, D. I. Sharapa, C. Schubert, D. Zahn, M. Halik, P. A. Keller, S. G. Pyne, S. Jennepalli, D. M. Guldi and T. Clark, *J. Am. Chem. Soc*., 2014, **136**, 10890.
35 J. Tuček, K. C. Kemp, K. S. Kim and R. Zbořil, *ACS Nano*, 2014, **8**, 7571.
36 S. M. Falke, C. A. Rozzi, D. Brida, M. Maiuri, M. Amato, E. Sommer, A. D. Sio, A. Rubio, G. Cerullo, E. Molinari and C. Lienau, *Science*, 2014, **344**, 1001.
37 A. Rao, P. C. Y. Chow, S. Gélinas, C. W. Schlenker, C.-Z. Li, H.-L. Yip, A. K.-Y. Jen, D. S. Ginger and R. H. Friend, *Nature*, 2013, **500**, 435.
38 S. Kirner, M. Sekita and D. M. Guldi, *Adv. Mater*., 2014, **26**, 1482.
39 M. Vizuete, M. J. Gómez-Escalonilla, J. L. G. Fierro, K. Ohkubo, S. Fukuzumi, M. Yudasaka, S. Iijima, J.-F. Nierengarten and F. Langa, *Chem. Sci*., 2014, **5**, 2072.
40 Z. C. Hu, B. J. Deibert and J. Li, *Chem. Soc. Rev*., 2014, **43**, 5815.
41 J. P. Huo, L. T. Fang, Y. L. Lei, G. C. Zeng and H. P. Zeng, *J. Mater. Chem. A*, 2014, **2**, 11040.
42 J. P. Huo, G. H. Deng, W. Wu, J. F. Xiong, M. L. Zhong and Z. Y. Wang, *Macromol. Rapid Commun.*, 2013, **34**, 1779.
43 J. P. Huo, J. C. Luo, W. Wu, J. F. Xiong, G. Z. Mo and Z. Y. Wang, *Ind. Eng. Chem. Res*., 2013, **52**, 11850.
44 J.-G. Cai, Z.-T. Yu, Y.-J. Yuan, F. Li and Z.-G. Zou, *ACS Catal*., 2014, **4**, 1953.
45 Z.-D. Meng, T. Ghosh, L. Zhu, J.-G. Choi, C.-Y. Park and W.-C. Oh, *J. Mater. Chem*., 2012, **22**, 16127.
46 Y.-J. Yuan, Z.-T. Yu, H.-L. Gao, Z.-G. Zou, C. Zheng and W. Huang, *Chem.-Eur. J*., 2013, **19**, 6340.
47 B. Zhu, H. X. Chen, W. Lin, Y. Ye, J. Wu and S. J. Li, *J. Am. Chem. Soc*., 2014, **136**, 15126.
48 P. N. Kumar, R. Narayanan, M. Deepa and A. K. Srivastava, *J. Mater. Chem. A*, 2014, **2**, 9771.
49 Q. Zhang, Y. H. Gao, S. Y. Zhang, J. Y. Wu, H. P. Zhou, J. X. Yang, X. T. Tao and Y. P. Tian, *Dalton Trans*., 2012, **41**, 7067.
50 K. Chang, Z. W. Mei, T. Wang, Q. Kang, S. X. Ouyang and J. H. Ye, *ACS Nano*, 2014, **8**, 7078.
51 B. Chai, X. Liao, F. K. Song and H. Zhou, *Dalton Trans*., 2014, **43**, 982.
52 D. Bao, P. Gao, X. D. Shen, C. Chang, L. Q. Wang, Y. Wang, Y. J. Chen, X. M. Zhou, S. C. Sun, G. B. Li and P. P. Yang, *ACS Appl. Mater. Interfaces*, 2014, **6**, 2902.
53 J. G. Yu, B. Yang and B. Cheng, *Nanoscale*, 2012, **4**, 2670.
54 P. Kumar, B. Sain and S. L. Jain, *J. Mater. Chem. A*, 2014, **2**, 11246.
55 D. Saha and S. G. Deng, *Langmuir*, 2011, **27**, 6780.
56 H. B. Fu, T. G. Xu, S. B. Zhu and Y. F. Zhu, *Environ. Sci. Technol*., 2008, **42**, 8064.
57 Q. Li, B. D. Guo, J. G. Yu, J. R. Ran, B. H. Zhang, H. J. Yan and J. R. Gong, *J. Am. Chem. Soc.*, 2011, **133**, 10878.
58 F. He, G. Chen, Y. G. Yu, S. Hao, Y. S. Zhou and Y. Zheng, *ACS Appl. Mater. Interfaces*, 2014, **6**, 7171.
59 F. Y. Wen and C. Li, *Acc. Chem. Res*., 2013, **46**, 2355.
60 M. Beley and P. C. Gros, *Organometallics*, 2014, **33**, 4590.
61 Y. T. Lua, D. D. Wang, Z. G. Mou, J. Huang, Y. K. Du and P. Yang, *Colloids Surf. A: Physicochem. Eng. Aspects*, 2014, **457**, 282.
62 G. S. Li, B. Jiang, X. Li , Z. C. Lian, S. N. Xiao, J. Zhu, D. Q. Zhang and H. X. Li, *ACS Appl. Mater. Interfaces*, 2013, **5**, 7190.
63 X. J. Bai, L. Wang and Y. F. Zhu, *ACS Catal*., 2012, **2**, 2769.
64 F. Li, G. P. Chen, J. H. Luo, Q. L. Huang, Y. H. Luo, Q. B. Meng and D. M. Li, *Catal. Sci. Technol*., 2013, **3**, 1993.
65 M. Y. Wang, D. J. Zheng, M. D. Ye, C. C. Zhang, B. B. Xu, C. J. Lin, L. Sun and Z. Q. Lin, *Small*, 2015, *in press* (DOI: 10.1002/smll.201402692).
66 X. X. Yao, T. Y. Liu, X. H. Liu and L. D. Lu, *Chem. Eng. J*., 2014, **255**, 28.
67 M. Y. Wang, L. Sun, Z. Q. Lin, J. H. Cai, K. P. Xie and C. J. Lin, *Energy Environ. Sci*., 2013, **6**, 1211.
68 D. Placencia, W. N. Wang, R. C. Shallcross, K. W. Nebesny, M. Brumbach and N. R. Armstrong, *Adv. Funct. Mater*., 2009, **19,** 1913.
69 M. Y. Wang, L. Sun, J. H. Cai, P. Huang, Y. F. Su and C. J. Lin, *J. Mater. Chem. A*, 2013, **1**, 12082.
70 M. D. Ye, J. J. Gong, Y. K. Lai, C. J. Lin and Z. Q. Lin, *J. Am. Chem. Soc*., 2012, **134**, 15720.
71 J. R. Ran, J. Zhang, J. G. Yu, M. Jaroniec and S. Z. Qiao, *Chem. Soc. Rev*., 2014, **43**, 7787.